Revised Manuscript for No. admt.202000341

Wireless Multi-Stimulus-Responsive Fabric-based Actuators for Soft Robotic, Human-Machine Interactive and Wearable Applications

*Rong Yin, Bao Yang, Xujiao Ding, Su Liu, Wei Zeng, Jun Li, Su Yang, Xiaoming Tao**

Dr. R. Yin, Dr. B. Yang, X.J. Ding, S. Liu, Dr. W. Zeng, J. Li, S. Yang, and Prof. X. M. Tao
Research Center of Smart Wearable Technology, Institute of Textiles and Clothing, The Hong Kong Polytechnic University, Hong Kong, P. R. China

Dr. R. Yin
Wilson College of Textiles, North Carolina State University, Raleigh, NC 27606, U.S.A.

E-mail: xiao-ming.tao@polyu.edu.hk

Highlights:

- Driven by multiple sources of magnetic, optical, electrical, and thermal stimuli, a light-weight fabric-based bimorph actuator demonstrated for the first time
- Simple, speedy, and low-cost mass fabrication method with conductive fabric and biaxially oriented polypropylene film
- Wirelessly driven prototypes of a soft gripper, kickers, and artificial blooming fabric flowers

Keywords: Multi-stimulus-responsive actuator; fast response; fabric-based actuator; wireless-control; soft robotics

Abstract:

Soft actuators driven by pneumatic or electric means are clumsy and heavy with physical connections, which hinders their robotic applications in the human-machine interactive, wearable, and biomedical fields. To overcome these shortcomings, a light-weight, soft remotely-controlled fabric-based actuator is presented. It can be driven by multiple wireless sources including optical, thermal, and magnetic stimuli. The bimorph actuator is fabricated by laminating electrically conductive fabric and biaxially oriented polypropylene film. The demonstrated prototypes show a large bending deformation (the curvature up of 0.75 cm^{-1} with the optical stimulus and 0.55 cm^{-1} with the magnetic stimulus). A fast response (0.27 s) with an angle of 100 ° from flat to the campulitropal shape can be achieved with the magnetic stimulus, more than twice faster than previously reported bimorph actuators. The remarkable performance of the actuators is attributed to the optimal structural design based on a verified model given by Timoshenko, good electrothermal properties and excellent optical absorption of the conductive fabric enhanced by copper/nickel coating. More importantly, it is greatly enhanced by the large difference of thermal expansion coefficients between the biaxially oriented polypropylene film and the conductive fabric. Various biomimetic and wireless controlled prototypes are demonstrated, such as a soft gripper, soft kickers, and artificial blooming flower, illustrating a new way to mass produce cost-effective bimorph actuators via a simple and fast approach for practical biomimetic applications in robots, wearable and functional textiles.

1. Introduction

Soft actuators are being increasingly pursued in bio-applications in robotics, artificial muscles, and biomimetic devices, due to their low reactive force, flexibility and capacity of large deformation and complex motion.[1] Unlike conventional motors and pneumatic linear or rotary actuators that typically consist of rigid elements and complex structures, soft actuators composed of elastic and lightweight materials can achieve complex motions in a relatively simple way.[1] Among various actuating structures, bimorph structure has drawn significant attention to generate bending motion via asymmetric deformation of the two layers, an active layer that contracts or expands by an external stimulation and a passive layer that remains intact.[2] Large curvature up to 2.6 cm^{-1}[3] and bending angle of 479°[4] as well as sophisticated biomimetic motions such as walking[5], swimming[6], rolling[4] and jumping[1] have been achieved through proper design of the bimorph structure.

The soft actuators can be activated by various external stimuli such as electricity [3, 5, 7], heat[8], light[1, 4, 7f, 9], magnetism[6, 10], induction heating[11], and moisture[2, 12]. The electrically stimulated one requires physical connection of electric wires between the actuators and power supply. Pneumatic actuators also have clumsy pipes and pumps connected[13]. In biomedical, human-machine reactive and wearable applications, light weight, wireless actuation, and remote control of the actuators are highly desirable or essential in some cases. There are numerous approaches that can achieve the remote actuation and wireless control according to the physical properties of the actuating materials employed in the soft actuators. For example, the radiation from an external

light source is one of widely and conveniently used stimulus. However, up to now, achieving good performance of light powered actuators has been challenging even in the outdoor sun.[9d] And such devices have even lower energy conversion efficiency at night and cloudy day. Magnetic soft actuators are programmed by changing the magnitude and direction of the magnetism [6, 10]. Induction heating driven actuators are thermo-responsive and electric-conducting actuators which are heated by eddy currents generated through electromagnetic induction [14]. The above actuators only react to single stimulus. Such methods possess limitations in performance and controllability in comparison to systems based on multiple stimuli. And thus, some multi-stimuli-responsive actuators have been developed, such as light and heating responsive actuator[9c], light and heating driven actuator[12b], electricity and sunlight driven actuator[1], and electricity and humidity driven actuator[2]. However, electromagnetic stimulus, possessing extreme merits in the programed direction and amplitude as well as motion control, has not been developed with other stimuli for a multi-stimulus-responsive actuator, which can mimic advanced and sophisticated biological movements even in a complex environment with barriers. Because magnetic field can penetrate most of barriers easily. Moreover, Textile materials with woven, knitted, and nonwoven structure have gained increasing interests for soft robotic, human-machine interactive, and wearable applications due to their soft and flexible nature, anisotropic properties, and hierarchical structure. For example, Hubbard et al.[15] proposed a solvent-responsive actuator by combining hydrogels with elastomers via a woven fabric interface. The woven fabric improves the mechanical properties of the actuator and

bounds two different materials without chemical treatment. Jiang et al.[16] presented a temperature-triggered nonwoven actuator. Both the thermo-responsive Poly (N-isopropylacrylamide) and passive thermoplastic polyurethane were electro-spun into nanofiber nonwoven mats with high surface area and porosity. Shin et al.[17] studied a humidity-responsive ratcheted robot with nonwoven polyethylene oxide nanofibers active layer attached to a polyimide thin film. Wang et al.[18] harnessed hygroscopic behavior of tractable microbial cells to design sweat-responsive wearables using a passive knit component. And these textile-based actuators have not been multi-stimulus-responsive.

Different expansion of the active and passive layer leads to a bending deformation when the applied temperature changes, which is the essential mechanism of the bilayer actuators. It is necessary that large difference between the coefficient of thermal expansion (CTE) of the active and that of the passive layer and effective heat transfer in the bilayer actuators for a large deformation. And thus, material selection is one of the most important design considerations. Carbon nanotube [5, 7b-d, 9a, 9c], graphene/reduced graphene oxide [4, 7a, 7f, 9b, 12b], and silver nanoparticles/nanowires [3, 7e] based films have been extensively investigated as a passive layer as well as an flexible heater due to their low CTE, suitable elastic modulus as well as thermal and electrical conductivities. However, these materials usually require either high electrical voltage or current for activation, which makes them very challenging for biomimetic applications in addition to causing safety issues. Moreover, these nanomaterials are expensive [19] and some of them have toxicity issues[20], which prevents their massive

production. Poly(dimethylsiloxane) has also been frequently employed as the active layer due to a high positive CTE [1, 3-4, 7a-c]. Yet, its elastic modulus is low (from several MPa to hundreds of kPa), normally leading a mismatch of bending stiffness between the poly(dimethylsiloxane) layer and the passive layer. As a result, a small actuation curvature was achieved with high activated temperature beyond 100 ºC and a long heating and cooling time [21]. Therefore, it remains a grand challenge to high performance soft actuators with large curvature under a relative low temperature via a facile, safe, cost-effective, and mass-produced approach.

Comparing to ionic diffusion and moisture, heat is the mostly utilized stimulus in the applications of soft actuators because it is fast and convenient to generate heat for bending and dissipate heat for recovery. Heat inside the bilayer actuator can be generated through heat transfer from environment, radiation from external light sources, and electric current from external power supply or induction of alternating magnetic field. Aiming to achieve a large curvature induced by thermo-expansion, apart from selection of materials with large CTE difference and effective heat transfer, the heat generated inside the actuator also is essential for many cases via a wireless method. Therefore, it is desirable to develop an actuator with a multifunctional layer which play dual roles of the active/passive layer and a wireless heat source. Moreover, from the theoretical model derived by Timoshenko[21], optimal structural design of the actuator is necessary because its curvature relies on elastic modulus, thickness, thickness ratio of the layers.

Here, we present a new approach to design and fabricate soft biomorph actuators by

laminating a conductive fabric (CF) and biaxial oriented polypropylene (BOPP) film for the first time. The resultant actuators demonstrate large and fast wireless actuations under multiple stimuli, by appropriate structural design. Upon electromagnetic stimulus, it shows bending actuation from flat to an arc shape with a curvature of ~ 0.55 cm^{-1} in 4 s and an angle of 100 ° from flat to campulitropal shape in 0.27 s, whereas simulated sunlight-induced deformation with a curvature of 0.75 cm^{-1} in 1.6 s can be achieved. These remarkable actuation performances are mainly attributed to the optimal structural design, excellent properties of stably electric-thermal, optical absorption and thermal conductivity brought by the conductive coating, and large CTE difference between two different layers. Based on the proposed soft actuators, we demonstrated various biomimetic motions of artificial blooming flower, soft kicker, and soft mechanical gripper as prospecting soft robots, wearable and functional textiles.

2. Results and Discussion

In this study, a novel soft actuator comprises a biaxially oriented polypropylene (BOPP) film and a conductive fabric (CF) layer, which are laminated by acrylic glue. Being a roller pressing machine, the laminating process of the actuator at room temperature is simple, ultrafast, and no water or solvent is required, as shown in **Figure 1a**. The BOPP film with a thin acrylic glue layer, that is a commercial adhesive tape, was selected to be an active layer due to its merits of high thermal expansion, lightweight, low-cost, and large quantities. The CF layer, also a mature commercial product made of conductive polyethylene terephthalate (PET) filaments, plays dual

roles of a passive layer and a soft heater. The PET filaments were first chemical plated with nickel and then electroplated with copper and nickel before woven into fabric. A cross-section of the suggested actuator (**Figure 1b**) show that the thickness of the BOPP film with an acrylic layer is ~ 55 μm, and the thickness of PET filaments with a conductive coating layer is ~ 35 μm. And the thickness of the conductive coating is ~ 900 nm. Moreover, the acrylic glue bounds the surface of CF fully with excellent flexibility. In this paper, the thickness of the fabricated actuator is 90 μm without mentioning. As shown in **Figure 1c**, a large-size actuator has been produced by feeding 5 BOPP films parallelly and a large size CF into the roller pressing machine at room temperature, showing that the actuator can scale up easily for industrial production. The actuation motion of the fabricated actuator was mainly attributed to the mismatch in thermal expansion between two layers during heating and cooling processes. As shown in **Figure 1d**, the fabricated actuator responses to multiple stimuluses, including electricity and magnetism, heat, electricity, and light, due to merits of the CF layer like high thermal coefficient, excellent light absorption, and good conductivity.

The dimensional change of the BOPP film and the CF were measured carefully by using a thermomechanical analysis device (Mettler Toledo TMA/SDTA1, Switzerland), showing that the dimensional change, that is strain, of these materials is a function of temperature (**Figure 2a**). The slope of the curves represents the CTE which increases with the raise of the applied temperature. The largest CTE can be obtained from the BOPP film in the longitudinal direction, and the smallest CTE is got from the CF in the warp direction. For example, at 40 ºC, the CTE of BOPP film is 124×10^{-6} K^{-1} in the

longitudinal direction and $46\times10^{-6}\,K^{-1}$ in the width direction, respectively, and the CTE of CF is $5\times10^{-6}\,K^{-1}$ and $15\times10^{-6}\,K^{-1}$ in the warp and the weft direction, respectively. Thus, the fabricated actuator comprises the CF in the warp direction and the BOPP film in the longitudinal direction, achieving the largest $\Delta\alpha$. Moreover, the thermal conductivity of the pristine PET fabric with copper/nickel coating, that is CF, and without coating across the thickness and warp directions were also investigated carefully. As illustrated in **Figure 2b**, a pristine PET fabric without coating has similar the thermal conductivity across the thickness (0.17 W/mK) and warp direction (0.23 W/mK), closes to that of the pure PET film (0.19 W/mK) [22]. Comparing the thermal conductivity of pristine PET fabric without coating, the thermal conductivity of CF has a two orders increasement in amplitude, such as 4.22 W/mK across the thickness direction and 2.11 W/mK across the warp direction, indicating that the copper/nickel coating can effectively enhance the thermal conductive of the PET fabric, which is highly beneficial to achieve uniform bending of the actuator. Therefore, the actuator was fabricated based on a careful design, as shown in **Figure 2c**.

The curvature, κ, of the fabricated actuator can be approximately predicted by the following equation derived by Timoshenko[21].

$$\kappa = \frac{c\cdot\Delta\alpha\cdot\Delta T}{h} \tag{1}$$

where $c = 6\frac{(1+m)^2}{3(1+m)^2+(1+mn)(m^2+\frac{1}{mn})}$, is determined by the structural parameters and material properties of the bilayer; $m = t_1/t_2$ and $n = E_1/E_2$ are the ratio of thickness and Young's modulus of two layer, respectively; t_1 and t_2 are the thickness of the passive layer and the active layer, respectively; E_1 and E_2 are the Young's modulus of the passive layer and the active layer, respectively; h is the total thickness

of the actuator; $\Delta\alpha$ is the difference between the CTE of the active layer and that of the passive layer; and ΔT is the temperature difference from the fabricated temperature. There are several assumptions utilized in the above equations, including (1) the BOPP film and the CF layer are uniform in the term of thickness and the CTE, (2) there is an excellent bonding between the BOPP film (~ 55 μm) and the CF layer (~ 35 μm), as well as the thickness of the acrylic glue layer (~ 900 nm) can be neglected, (3) the bending of the bilayer along the transverse direction will be neglected, because the CTE difference between the BOPP in the longitudinal direction and the CF in warp direction is much larger than that between the BOPP in the transverse direction and the CF in the weft direction, as shown in **Figure 2a**, (4) the temperature of the actuator changes uniformly, (5) the CTEs are constant when the applied temperature changes, and (6) the materials utilized in actuator are linear-elastic materials, that is, the Young's modulus is constant during deformation. The stress-strain curves of the BOPP film and the CF were measured at different directions, respectively, indicating a linear relationship between stress and strain at the beginning stage of loading (**Figure S2**). The linear ranges are much larger than those induced by the temperature difference shown in **Figure 2a**. And thus, the Young's modulus of these materials can be calculated within the linear range. Then, the parameter of n is obtained as 1.77 (**Table S1**), which is defined as the ratio between Young's modulus of CF in the warp direction and that of the BOPP film in the longitudinal direction. Though some assumptions like uniform temperature changes, constant CTE and constant Young's modulus cannot satisfy strictly in the tests, it may still make an approximate prediction of curvature.

To verify the model, three sample of the actuators were fabricated with 40 mm in length and 10 mm in length. And then, they were tested at different temperatures by using a chamber with a glass window (**Figure S3**). The temperature of the chamber can be controlled with a precision of ~ 1℃. One end of the samples was fixed (shown in **Figure S3**). And then, the chamber was heated to the given temperature and holding for

5 minutes so that the temperature of the actuator became uniform, meanwhile, the bending of the actuator was recorded by a camera. The curvatures of the actuators are illustrated in **Figure 2d,** showing that larger curvature was obtained at a high temperature within the studied temperature range. And the parameters utilized to predict the curvature are listed in **Table S1**, which are consistent with the fabricated samples. The curvatures predicted by the model has an excellent agreement with the experimental results at the temperature from 33 ºC to 50 ºC, but slightly higher than those at the temperature of 55 ºC, 60 ºC and 65 ºC (**Figure 2d**). Because the thermal expansion difference, $\Delta\alpha$, increases with raising the temperature. Overall, this model can make a good prediction on the curvature of the fabricated actuator, and consequently, this model can be a powerful to guide the design of the actuator.

As shown in Equation (1), the curvature (κ) is proportional to c. When h, ΔT and $\Delta\alpha$ are given, a higher value of c will result in a larger curvature. And thus, the largest c is highly desirable to be achieved. As shown in **Figure 2e**, these curves indicate that a highest value of constant (~ 1.5) can be achieved by matching the parameter of m and n. When n is determined, there is an optimized m for achieving the highest value of c. Furthermore, as shown in **Figure 2f**, the relationship of the optimized m and n, that is, $m = {}^{1}/_{\sqrt{n}}$, can be powerful tool to guide the structural design when Young's modulus of the components is given. And the derivation of the optimized m is shown in the supporting information **S1**.

From the plotted curve marked in blue, corresponding to the utilized materials of the

BOPP film and the CF, the structural parameter of m is selected to be 1.57 for achieving the high value of c (~ 1.3, close to the highest value of 1.5). This key parameter of c is much larger than the previously reported actuators, such as 0.49 for Spongy graphene/Polydimethylsiloxane [7a] and about 0.01 for low-density Polyethylene /silver nanowire/Polyvinyl chloride [7e] and super-aligned carbon nanotube /Polyethylene terephthalate/BOPP [7d]. Moreover, the CF also is a good absorber of light due to multilevel structure of fabric and the metal coating. And the initial status of the actuator at room temperature can be easily controlled by adjusting the temperature of the roller during production (**Figure S1**). Therefore, from these merits of excellent electrical, thermal and light absorption properties and large thermal expansion difference between the active and passive layers, the fabricated actuator can response to multiple stimulations and have large bending deformation.

To illustrate a wireless multi-stimulus-responsive actuator, a strip BOPP/CF actuator was fabricated and tested. **Figure 3** exhibits the electromagnetically induced actuation of the fabricated actuator. As shown in **Figure 3a**, a fabricated actuator sample was laid flat on a barrier (a common A4 paper) over a magnetic field generator. The magnetic field generator (Figure **S5a**) can convert direct current (DC) from a power supply to an alternating current signal via oscillators as well as generating a high frequency alternating magnetic field across the coils. And such alternating current magnetic fields can induce an induction current and generate heat in the CF layer as an electromagnetic stimulus to the fabricated actuator. The bending profile and the temperature distribution

on the top surface were recorded by a camera and an infrared camera simultaneously, respectively. In this paper, the strip sample has a size of 40 mm in length and 10 mm in width so that its actuation and the temperature distribution can be conveniently measured by both cameras. The sample was heated from room temperature (**Figure 3b**). After heating, the actuator has an arc bending (**Figure 3c**). The bending process of the fabricated actuator induced by the alternating magnetic field is shown in **Figure 3d** and the video (**Video S1-1**). When the magnetic field generator turned on, the fabricated actuator bends form the initial status to a large bending angle (122 °) with had a fast response of ~ 3 s. And then, the device turned off, the bended actuator recovered to the initial status slowly (about 16.5 s required). The corresponding curvature changes with time are shown in **Figure 3e**, showing a large curvature ($1/R$) up to 0.53 cm^{-1}, where the bending angle and curvature are defining as **Figure 3c**. The max curvature is defined as the maximum curvature and the corresponding time is defined as the response time. The electromagnetically induced actuation under different DC voltages was also studied carefully (**Figure 3f**). A higher DC voltage can generator a larger amplitude of alternating magnetic field which makes a higher induction current in the CF layer as well as more heat generated in a shorter time. With the increase of the applied DC voltage, the response time are shortened form 7 s to 1.8 s, and the max curvature is increased from 0.2 cm^{-1} to 0.53 cm^{-1} and then declined. As shown in Figure **S5b**, the magnetic field inside the coil is remarkably uniform in magnitude and direction. However, the magnitude and direction of the magnetic field outside the coil will rely on the distance between the subject and the coil, showing that the magnitude of the

magnetic field become weak when the distance between the measured point and the coil increases. In our cases, the actuator is outside the coil, and the distances between the localized zone on the actuator and the coil are normally different from each other. It means that the generated heat on the CF is uneven. And thus, the highest temperature happens at the two sides of the middle part (**Figure 3c**), induced by nonuniform alternating magnetic field. The maximum local temperature increased from 40 ℃ to over 100 ℃ when the applied voltage increase from 20 V to 70 V. Moreover, the actuator needs to overcome the self-weight continually before achieving the max curvature. Therefore, the alternating magnetic field with uniform distribution and suitable amplitude changes which rely on the match of heat generating and heat conduction of the actuator. Though non-uniform alternating magnetic field, generated by a single group of coils, was illustrated and utilized in this work, uniform alternating magnetic field can be generated by multi-groups of coils easily. For example, a Helmholtz coil can produce a region of nearly uniform magnetic field [23]. Moreover, if the actuator sample was fixed at one end, and its top surface is perpendicular to the main direction of the magnetic field (**Figure S4**), the response time are sharply shortened to 0.27 s with an angle of ~100 º from flat to campulitropal shape.

The fabricated actuator also can be driven by light. To illustrate this, a simple system, including light, a clamp for fixing of the sample, a camera for recording the bending and an infrared camera for recording the temperature distribution, and a fabricated sample were setup (**Figure 4a**). As shown in **Figure 4b**, the initial state of the sample clamped at one end shows that there is a slight upward-bending due to the initial stress

state induced during the fabrication and cutting. Here, a simulated sunlight was applied as the light stimulus. Driven by an incident light irradiation from the top-left side, the actuator bended promptly to the curved shape with a curvature change from the initial state to a large bending, θ, up to 95 ° (**Figure 4c** and **Video S1-2**)). Meanwhile, the max temperature of the sample changes from 27.9 ℃ to 66.6 ℃. As shown in **Figure 4d**, the actuator bended from the initial state close to a horizontal film to 0.75 cm^{-1} within 2.73 s under a light intensity of 130 mW cm^{-2}, and then the light turned off, the sample recovered to the initial state with 11.70 s required. Achieving a similar max curvature, the response time can greatly shorten with raising the light intensity (**Figure 4e**). While the max curvature remains ~ 0.75 cm^{-1}, the response time can shorten from 11.43 s to 1.60 s when the light intensity increases from 50 mW cm^{-2} to 230 mW cm^{-2}. The end forces of the actuator also evaluated and shown in **Figure 4f**, indicating that the force increases (up to 1 mN) with increasing temperature from 22 ℃ to 57 ℃. Moreover, as shown in **Figure S6a**, the bending movements of four actuators with a same length-width ratio (3:1) shows that all the actuators have a similar resultant curvature at the same light stimulation. And the force increases with an increasement in width (**Figure S6b**). These results indicate that the bending moment or force can be adjust by changing the aspect ratio and the width of the actuator. For comparison of the actuation of the BOPP/CF actuator, a BOPP/PET actuator made of the BOPP film and the pure PET fabric was fabricated and tested (**Figure 4g**). Under same light intensity of 130 mW cm^{-2}, the BOPP/ PET actuator shows a smaller curvature (0.1 cm^{-1}) than that of the BOPP/CF actuator (~ 0.8 cm^{-1}) and even much longer response time, which

implies the excellent photothermal properties played by the conductive coating. As shown in the video (**Video S1-3**), both actuators were tested together. And the result indicated that the BOPP/CF actuator has a faster response with an obviously larger curvature than that of the BOPP/PET actuator.

A summary of the reported electrothermal and photothermal active actuators is illustrated in **Table 1**, showing that the fabricated actuator outperforms the reported actuators in terms of the response time with a large deformation, such as a much shorter response time of 0.27 s, over two times faster than the reported soft actuators, with a large curvature of 0.40 cm^{-1} (**Figure S4e**) and the corresponding response rate up to 1.48 $cm^{-1}s^{-1}$ based on electromagnetic actuation, and a short response time of 1.6 s with a large curvature of 0.75 cm^{-1} and the corresponding response rate up to 0.469 $cm^{-1}s^{-1}$ based on the light actuation. The presented deformation did not show an extremely large curvature because the maximum temperature difference was restricted at about 40 ~ 50 ^{o}C and a relative thick actuator (90 μm). From Equation (1), a large curvature of such actuator can be achieved easily by reducing the total thickness.

The fabricated actuator with merits of fast response, multiple stimuluses, good flexibility, large deformation, and mild heating condition can be used to develop various wireless controlled devices toward practical applications. As a proof-of-concept, three wireless-controlled demonstrations, including a soft mechanical grasper, a soft kicker and acritical bloom flowers, were designed and shown in **Figure 5**. A soft mechanical grasper was driven by light to grasp a lightweight object. With controlling the light on and off, the soft grasper opens and closes to grab and put down the objective, as shown

in **Figure 5a** and the video (**Video S2-1**). A soft kicker was driven by magnetic signals to mimic that the leg motion to kick a ball (**Figure 5b** and **Video S2-2**). Due to the fast response of the fabricated actuator, a table tennis ball was pushed promptly and accelerated away from the actuator, like the behavior that a human leg kicks the ball. The weight of the utilized table tennis ball was about 6 times over that of the actuator, and the average moving speed of the table tennis ball was measured up to 122 mm/s. In a similar way, a smaller kicker driven by light was fabricated and tested, showing a slower moving speed of 74 mm/s and a higher ratio up to 27 times between the weight of table tennis ball and the actuator (**Figure S7** and **Video S2-3**). Moreover, a simple demonstration of an artificial blooming flower was designed and shown in **Figure 5c** and the video (**Video S2-4**). Such blooming flower was composed of 19 petals with 40 mm in length and 10 mm in width. The petals were initially flat. When an electromagnetic stimulation was applied, each petal will bend outward like a blooming flower, where the required time is 3.6 s from initial state to the blooming state at the power input of DC 48 V. Likewise, an advanced artificial blooming flower was fabricated with 2 layers of total 46 petals attached on a fashion cloth, as shown in **Figure 5d** and the video (**Video S2-5**). The petals were colored by spray cyan painting on the CF side. Under the light intensity of the sunlight about 100 mW cm^{-2}, the petals of flower curled like an attractive blooming artificial flower. These demonstrations show a new way for using low-cost commercial products based on a simple and ultrafast fabrication approach to construct soft actuators toward practical biomimetic application in robots and functional textiles.

3. Conclusion

Driven by multiple sources of light, magnetic, thermal, and electrical stimuli, a soft fabric-based bimorph actuator was developed by laminating a BOPP film and a conductive fabric at room temperature. The speedy and cost-effective production method facilitated mass production of the actuating fabrics of very large size. The fabric-based actuator can be controlled wirelessly, possessing an extremely fast response (0.27 s) with a large bending deformation (angle of 100^{o}), more than twice faster than previously reported bimorph actuators. On the other hand, a large arc bending with a curvature of 0.75cm^{-1} in 1.6 s and 0.55 cm^{-1} in 3 s was achieved by light radiation and magnetic stimulus, respectively.

These merits are attributed to the outstanding thermal and electrical conductivity of the CF layer, and more importantly, optimal design and the large difference of thermal expansion between the BOPP film and the CF. From the developed actuator, various biomimetic prototypes were demonstrated, including a soft mechanical gripper, soft kickers and artificial blooming flowers. The report work leads to a new way to mass produce cost-effective bimorph actuators via a simple and fast approach for practical biomimetic applications in robots, wearable and functional textiles.

4. Experimental Section

Preparation of CF/BOPP actuator: The commercial BOPP film (adhesive tape, 55 μm thickness, deli 30201, China) and conductive fabric (35 μm thickness, Kunshan EMS Electronic Material Co., China) were used without any post processing. The actuator

can be fabricated either by hand or with the help of a roller pressing machine (8350T, Haozhanyou Co., China). Demonstrations, including actuators, artificial flowers, soft kickers and graspers, were fabricated in the same way.

Fabrication of pristine PET fabric: The pristine PET fabric was obtained by removing the conducting coating of the CF. A solution with 6 g Iron (III) chloride and 0.5 ml 67% HNO_3, dissolved in 800 ml deionized water was prepared. Then 25 cm × 15 cm CF sample was immersed in the solution and treated with ultrasonic for 45 minutes. After the conductive coating was totally removed, the pristine PET fabric was rinsed and dried. The weight ratio of the conductive coating is 47.74%, measured by an electric balance by weighting the sample before and after treatment. The result is consistent with the result of TGA (**Figure S8**).

Characterization: An Infrared camera (FLIR systems, A645sc, America) was used to measure the temperature distribution on the top surface of the actuator. The BOPP film is at top without mentioning. The deformation of the actuator was captured by the digital camera in cell phone (Xiaomi 6). The forces of the actuator were measured by an electronic scale (Futek, LRF400, Finland). The CTEs of the CF and BOPP were measured by the thermomechanical analysis (Mettler Toledo TMA/SDTA1, Switzerland). Stress-strain curves of the CF and BOPP were tested by Kawabata evaluation system (Tensile & shear tester). The SEM images were obtained by Hitachi S-4800 field emission scanning electron microscope. ZVS high frequency induction heating device (Shenzhen Fengtai Electronic Technology Co., China) and a xenon lamp were used to provide electromagnetic and light stimulation. The thermal conductivity

values were tested by Hot Disk TPS2500S according to the standard of ISO220007-2 (Transient Plane Source Method).

Supporting Information

Supporting Information is available from the Wiley Online Library or from the author.

Acknowledgements

Dr. R. Yin and Dr. B. Yang contributed equally to this work. The authors acknowledge financial support from the Research Grants Council, Hong Kong (Project no. 525113, 15215214, 15211016, 15200917), Hong Kong Polytechnic University, Hong Kong (Project no. 1-BBA3), and Innovation and Technology Commission, Hong Kong SAR Government (Project no. ITP/039/16TP).

Conflict of Interest

The authors declare no conflict of interest.

References

[1] Y. Hu, J. Q. Liu, L. F. Chang, L. L. Yang, A. F. Xu, K. Qi, P. Lu, G. Wu, W. Chen, Y. C. Wu, *Advanced Functional Materials* **2017**, 27.

[2] M. Amjadi, M. Sitti, *Acs Nano* **2016**, 10, 10202.

[3] S. S. Yao, J. X. Cui, Z. Cui, Y. Zhu, *Nanoscale* **2017**, 9, 3797.

[4] Y. Hu, G. Wu, T. Lan, J. J. Zhao, Y. Liu, W. Chen, *Adv Mater* **2015**, 27, 7867.

[5] L. Z. Chen, M. C. Weng, Z. W. Zhou, Y. Zhou, L. L. Zhang, J. X. Li, Z. G. Huang, W. Zhang, C. H. Liu, S. S. Fan, *Acs Nano* **2015**, 9, 12189.

[6] W. Q. Hu, G. Z. Lum, M. Mastrangeli, M. Sitti, *Nature* **2018**, 554, 81.

[7] a) Y. Hu, T. Lan, G. Wu, Z. C. Zhu, W. Chen, *Nanoscale* **2014**, 6, 12703; b) Q.

W. Li, C. H. Liu, Y. H. Lin, L. Liu, K. L. Jiang, S. S. Fan, *Acs Nano* **2015**, 9, 409; c) Z. H. Zeng, H. Jin, L. P. Zhang, H. Zhang, Z. Chen, F. Gao, Z. Zhang, *Carbon* **2015**, 84, 327; d) L. Z. Chen, M. C. Weng, W. Zhang, Z. W. Zhou, Y. Zhou, D. Xia, J. X. Li, Z. G. Huang, C. H. Liu, S. S. Fan, *Nanoscale* **2016**, 8, 6877; e) H. Kim, H. Lee, I. Ha, J. Jung, P. Won, H. Cho, J. Yeo, S. Hong, S. Han, J. Kwon, K. J. Cho, S. H. Ko, *Advanced Functional Materials* **2018**, 28; f) Y. Y. Yang, M. Zhang, D. F. Li, Y. J. Shen, *Advanced Materials Technologies* **2019**, 4.

[8] a) M. Kanik, S. Orguc, G. Varnavides, J. Kim, T. Benavides, D. Gonzalez, T. Akintilo, C. C. Tasan, A. P. Chandrakasan, Y. Fink, P. Anikeeva, *Science* **2019**, 365, 145; b) X. J. Qian, Q. M. Chen, Y. Yang, Y. S. Xu, Z. Li, Z. H. Wang, Y. H. Wu, Y. Wei, Y. Ji, *Adv Mater* **2018**, 30.

[9] a) X. Zhang, Z. B. Yu, C. Wang, D. Zarrouk, J. W. T. Seo, J. C. Cheng, A. D. Buchan, K. Takei, Y. Zhao, J. W. Ager, J. J. Zhang, M. Hettick, M. C. Hersam, A. P. Pisano, R. S. Fearing, A. Javey, *Nature Communications* **2014**, 5; b) W. T. Jiang, D. Niu, H. Z. Liu, C. H. Wang, T. T. Zhao, L. Yin, Y. S. Shi, B. D. Chen, Y. C. Ding, B. H. Lu, *Advanced Functional Materials* **2014**, 24, 7598; c) X. B. Zhang, C. L. Pint, M. H. Lee, B. E. Schubert, A. Jamshidi, K. Takei, H. Ko, A. Gillies, R. Bardhan, J. J. Urban, M. Wu, R. Fearing, A. Javey, *Nano Letters* **2011**, 11, 3239; d) K. Kumar, C. Knie, D. Bleger, M. A. Peletier, H. Friedrich, S. Hecht, D. J. Broer, M. G. Debije, A. P. H. J. Schenning, *Nature Communications* **2016**, 7.

[10] a) R. Tognato, A. R. Armiento, V. Bonfrate, R. Levato, J. Malda, M. Alini, D. Eglin, G. Giancane, T. Serra, *Advanced Functional Materials* **2019**, 29; b) T. N. Do, H. Phan, T. Q. Nguyen, Y. Visell, *Advanced Functional Materials* **2018**, 28, 1800244.

[11] a) S. M. Mirvakili, D. Sim, I. W. Hunter, R. Langer, *Sci Robot* **2020**, 5; b) M. Boyvat, D. M. Vogt, R. J. Wood, *Adv Mater Technol-Us* **2019**, 4, 1800381 %@ 2365.

[12] a) X. H. Yang, W. H. Wang, M. H. Miao, *Acs Appl Mater Inter* **2018**, 10, 32256; b) J. K. Mu, C. Y. Hou, H. Z. Wang, Y. G. Li, Q. H. Zhang, M. F. Zhu, *Sci Adv* **2015**, 1; c) M. M. Ma, L. Guo, D. G. Anderson, R. Langer, *Science* **2013**, 339, 186; d) T. J. Jia, Y. Wang, Y. Y. Dou, Y. W. Li, M. J. de Andrade, R. Wang, S. L. Fang, J. J. Li, Z. Yu, R. Qiao, Z. J. Liu, Y. Cheng, Y. W. Su, M. Minary-Jolandan, R. H. Baughman, D. Qian, Z. F. Liu, *Advanced Functional Materials* **2019**, 29.

[13] Y. Sun, H. K. Yap, X. Liang, J. Guo, P. Qi, M. H. Ang Jr, C.-H. Yeow, *Soft robotics* **2017**, 4, 251.

[14] a) S. M. Mirvakili, D. Sim, I. W. Hunter, R. Langer, *Sci Robot* **2020**, 5; b) M. Boyvat, D. M. Vogt, R. J. Wood, *Advanced Materials Technologies* **2019**, 4, 1800381.

[15] A. M. Hubbard, W. Cui, Y. Huang, R. Takahashi, M. D. Dickey, J. Genzer, D. R. King, J. P. Gong, *Matter* **2019**, 1, 674.

[16] S. Jiang, F. Liu, A. Lerch, L. Ionov, S. Agarwal, *Adv Mater* **2015**, 27, 4865.

[17] B. Shin, J. Ha, M. Lee, K. Park, G. H. Park, T. H. Choi, K.-J. Cho, H.-Y. Kim,

Sci Robot **2018**, 3.

[18] W. Wang, L. Yao, C.-Y. Cheng, T. Zhang, H. Atsumi, L. Wang, G. Wang, O. Anilionyte, H. Steiner, J. Ou, *Sci Adv* **2017**, 3, e1601984 %@ 2375.

[19] J. K. Mu, M. J. de Andrade, S. L. Fang, X. M. Wang, E. L. Gao, N. Li, S. H. Kim, H. Z. Wang, C. Y. Hou, Q. H. Zhang, M. F. Zhu, D. Qian, H. B. Lu, D. Kongahage, S. Talebian, J. Foroughi, G. Spinks, H. Kim, T. H. Ware, H. J. Sim, D. Y. Lee, Y. Jang, S. J. Kim, R. H. Baughman, *Science* **2019**, 365, 150.

[20] N. Kobayashi, H. Izumi, Y. Morimoto, *J Occup Health* **2017**, 59, 394.

[21] S. Timoshenko, *JOSA* **1925**, 233.

[22] C. M. A. Lopes, M. I. Felisberti, *Polymer Testing* **2004**, 23, 637.

[23] a) A. E. Ruark, M. F. Peters, *JOSA* **1926**, 13, 205; b) S. Trout, *Ieee T Magn* **1988**, 24, 2108.

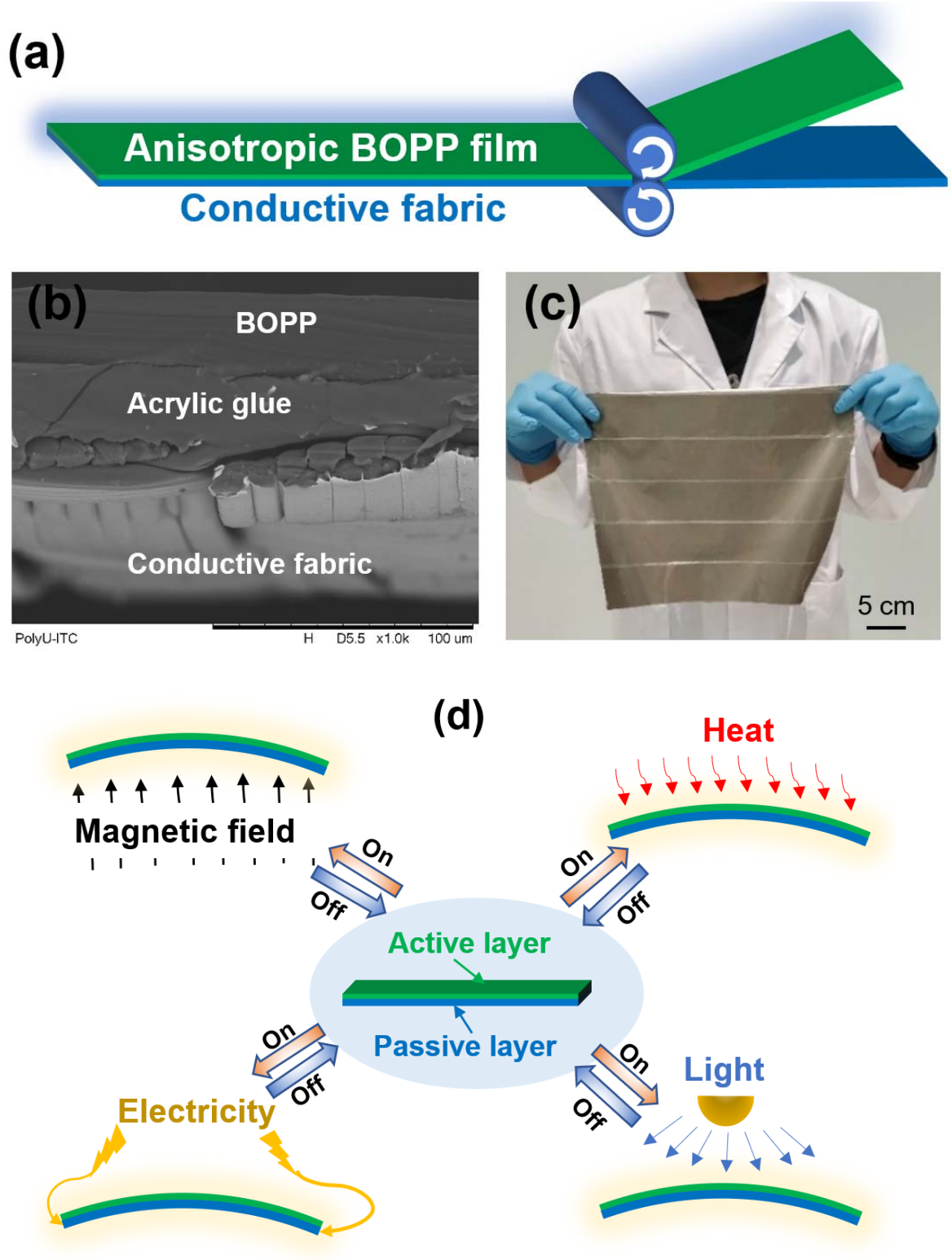

Figure 1. A soft fabric-based bimorph actuator. (a) Schematic of the lamination process of the actuator with a biaxially oriented polypropylene (BOPP) film as a thermally active layer and a conductive fabric as a thermal passive layer. (b) A cross-sectional SEM image of the actuator of a BOPP film laminated with a conductive fabric (acrylic as the adhesive). (c) Photo of a large-area actuating laminated fabric. (d) The actuator responds to multiple stimuli, including

three wireless stimuli: magnetic fields, heat, and light, as well as one wired stimulus: electricity.

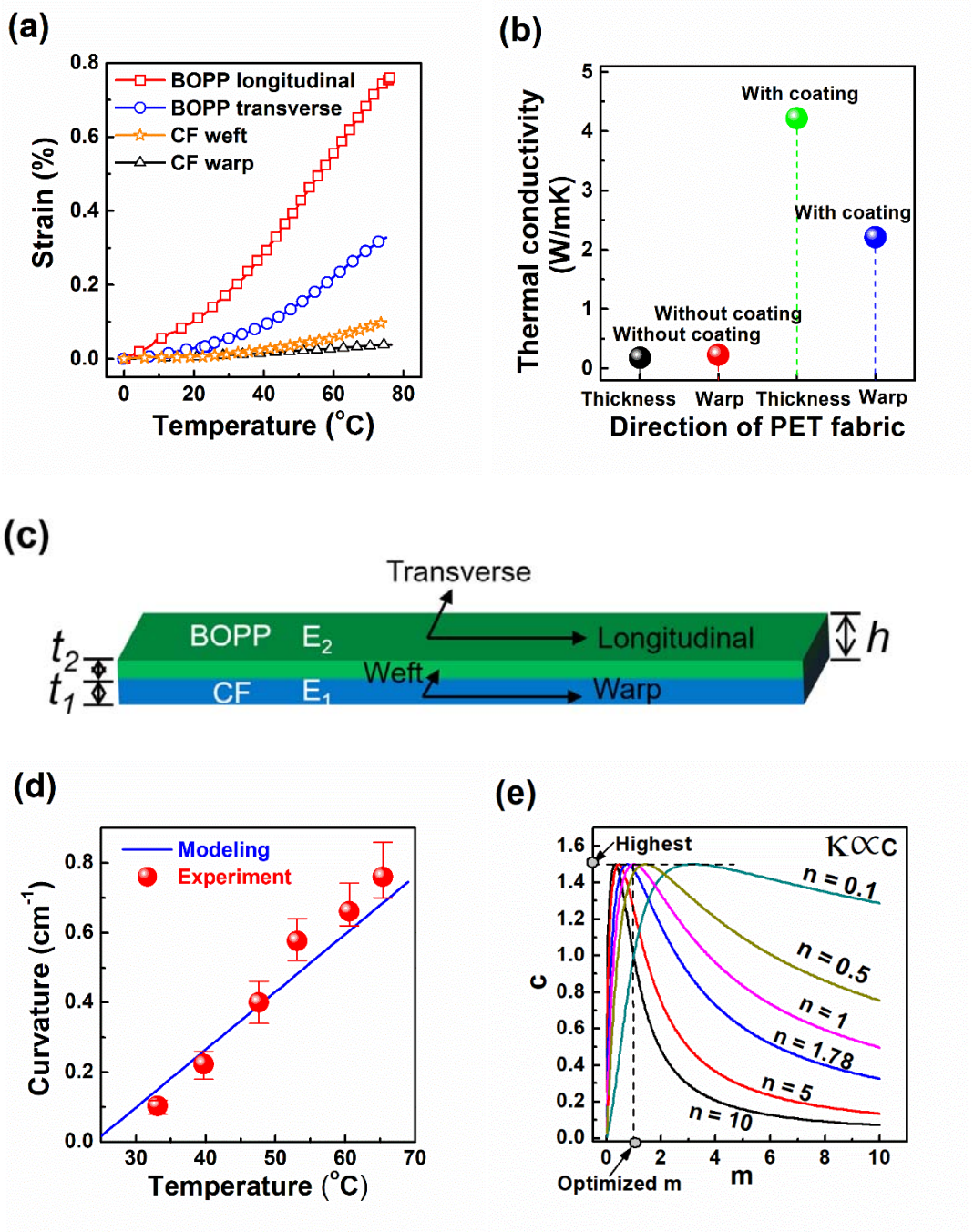

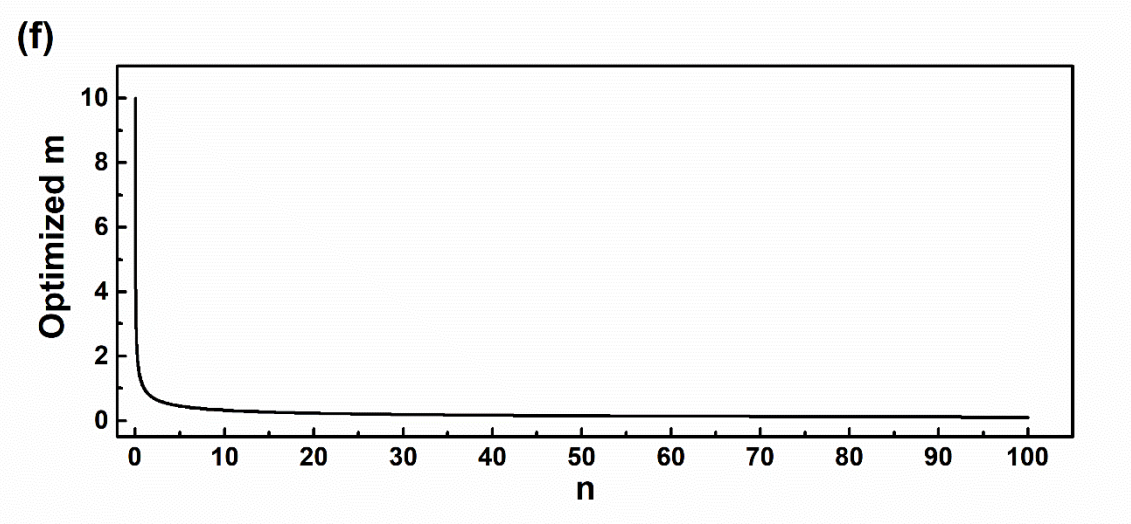

Figure 2. Material properties and design curves of the actuator. (a) Thermal expansion strain in the warp and weft directions of the conductive fabric (CF) and in the longitudinal and transverse directions of the BOPP film. (b) Thermal conductivity in the thickness and wrap direction of the copper/nickel coated PET fabric (CF) and PET fabric without coating. (c) Schematic of the fabricated fabric-based actuator. (d) Comparison between the curvatures calculated based on the Timoshenko's model and the experimental results of three fabricated samples, where the parameters utilized in calculation are listed in Table S1 and $\Delta\alpha$ is constant as 119 x10^{-6}/K close to that at 40 ^{o}C shown in Figure 2a. (e) Parameters c, proportional to the curvature, relies on the structural parameter of m and the material properties of n at a given thickness of h, indicating that the highest value of c can be achieved by adjusting m even at a different n. (f) Relationship between the given n and the optimized m for achieving the largest value of c.

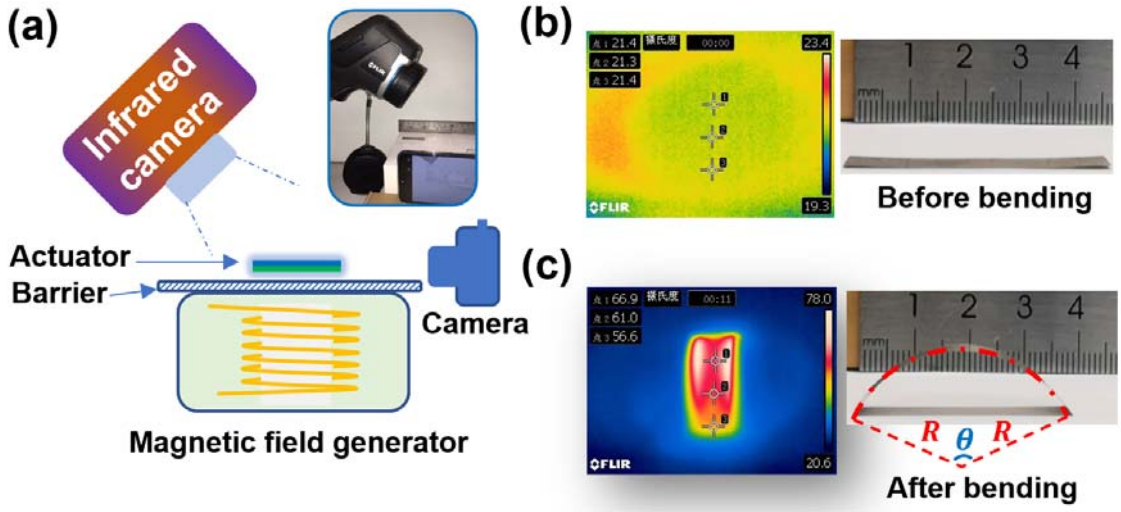

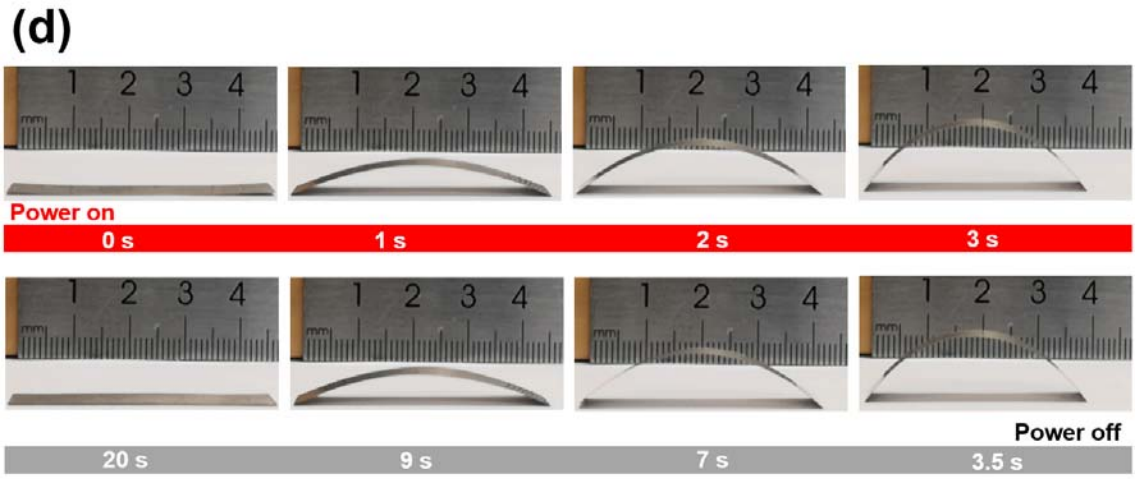

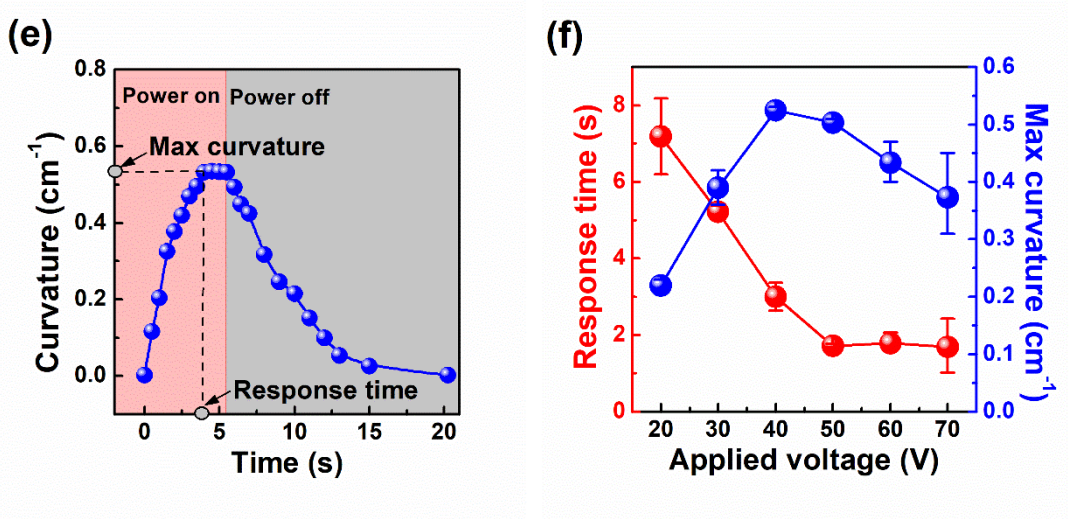

Figure 3. Actuation induced by alternating magnetic fields. (a) Schematic of the experimental setup and physical photo of devises, where the side view of the actuation process of the actuator was recorded by a camera, and the temperature distribution on the top side was recorded by an infrared camera simultaneously. (b) and (c) Illustrated temperature distribution of the top side and the corresponding bending profile of the actuator before and after deformation, respectively. (d) Electromagnetically induced actuation of a wireless-controlled actuator with 40 mm in length and 10 mm in width, and (e) Corresponding curvature of the fabricated actuator as a function of time, where the actuator flats on a A4 paper (an illustrated barrier) and the input DC voltage of magnetic field generator is 40 V. (f) Max curvature and the corresponding response time as a function of the input voltage.

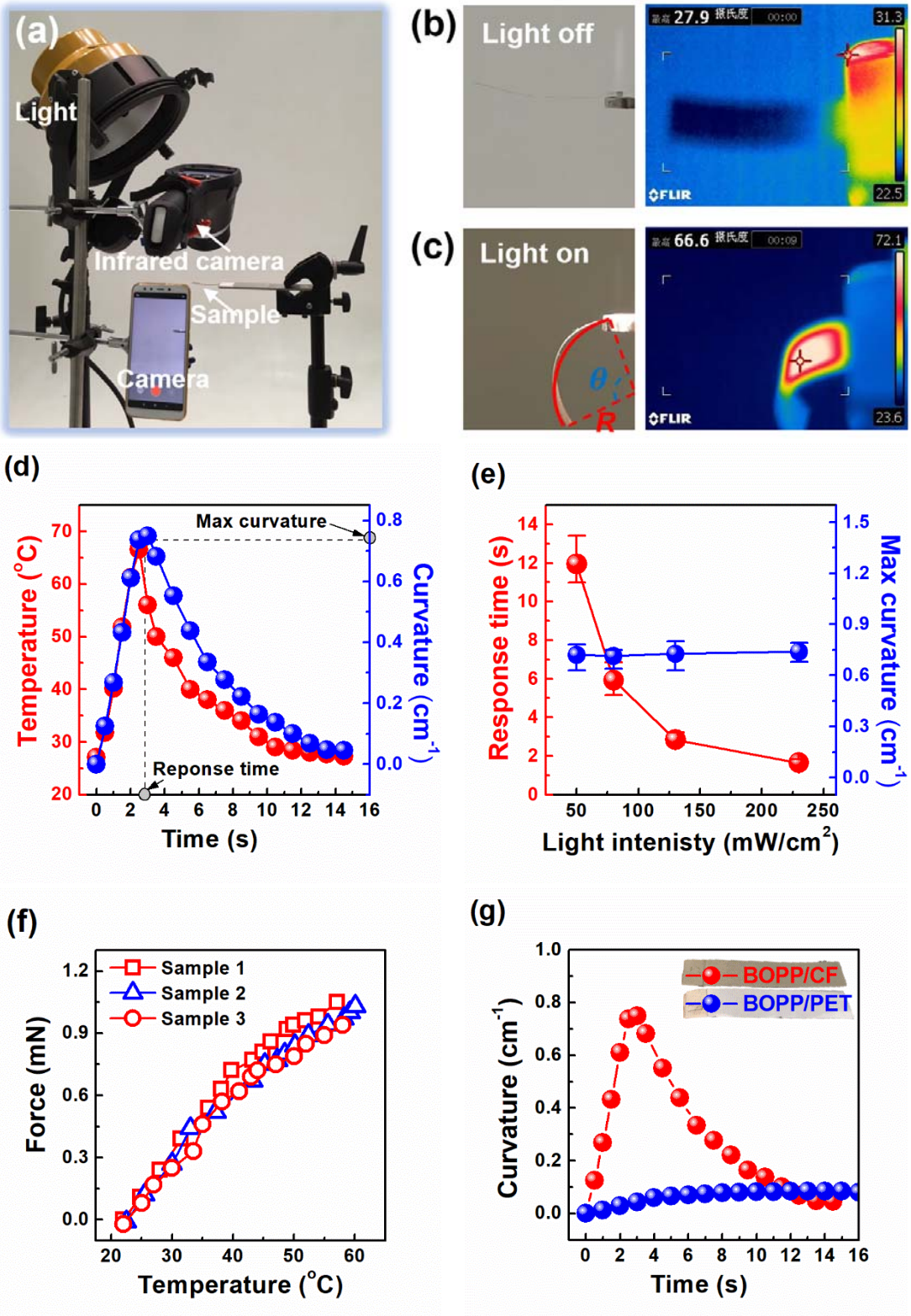

Figure 4. Light induced actuation of the actuator. (a) Photo of the measurement system, including a light for simulating sunlight, a clamp for fixing the sample, a camera for recording the deformation, and an infrared camera for recording the temperature distribution. (b) and (c) Side view optical images and infrared thermal images of the actuator before and after applying a light stimulation, respectively, where the sample is fabricated with a size of 40 mm in length and 10 mm in width and clamped at one end with a length of 5 mm. (d) Corresponding

temperature and curvature of the actuator as a function of time under the light intensity of about 130 mW cm^{-2}. (e) Response time of the actuator to the same curvature as a function of light intensity. (f) Blocking force of the actuator as a function of temperature. (g) Comparison of the actuation between the BOPP/CF actuator and the corresponding BOPP/PET actuator without conductive coating under the light intensity of about 130 mW cm^{-2}.

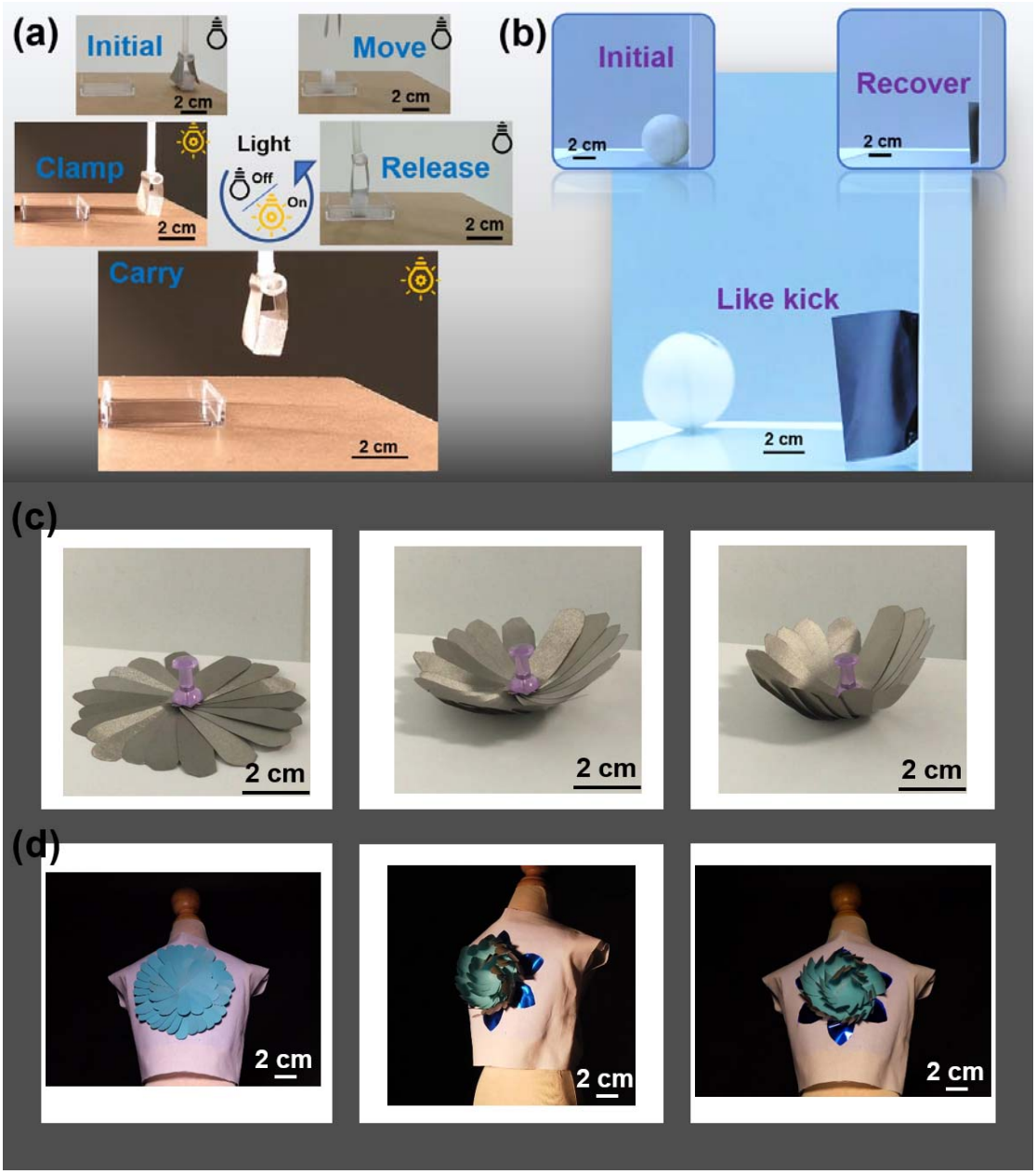

Figure 5. Wireless-activated demonstration of the BOPP/CF actuator. (a) A soft gripper driven by light: with the light on and off, the gripper opens and closes to grip and put down the object, where the gripper comprises 2 pieces of BOPP/CF actuators with 35mm x 35mm and a light intensity of about 130 mW cm^{-2} is employed. (b) A soft kicker driven by electromagnetic stimulation, which could mimic the leg motion to kick a table tennis ball. The sample size is 55 mm in length and 45 mm in width and the power input is DC 48 V. (c) Electromagnetically induced artificial blooming flower composed of 19 petals, where the size of the petals is 40 mm in length and 10 mm in length and the power input is DC 48 V. (d) A light driven artificial flower composed of 46 petals attached on a fashion cloth, where the sample size of the petals is 40 mm x 10 mm and a light intensity of about 100 mW cm^{-2} was employed. The actuators are colored by spray cyan painting on the CF side.

Table 1. Summary of the performance of reported bimorph actuators

Materials	Mechanism	Maximum curvature/ Bending angle	Response time (s) / Thickness (um)	Response rate	Maximum Temperature change (°C)	Input Power	Reference
PI/AgNW/PDMS	Electrothermal	2.6 cm^{-1}	~ 40/212.5	0.07 $cm^{-1}s^{-1}$	140	DC4.5 v	[3]
SACNT/PET/BOPP	Electrothermal	0.41 cm^{-1}	~ 30/120	0.05 $cm^{-1}s^{-1}$	50	DC 80 v	[7d]
SACNT/BOPP	Electrothermal	1.03 cm^{-1}	~ 10/47	0.10 $cm^{-1}s^{-1}$	37.6	DC 5 v	[5]
Spongy graphene/PDMS	Electrothermal	1.2 cm^{-1}	~ 3/130	0.40 $cm^{-1}s^{-1}$	80	DC 10 v	[7a]
LDPE/AgNW/PVC	Electrothermal	2.5 cm^{-1}	~ 30/40	0.08 $cm^{-1}s^{-1}$	22	142 mW	[7e]
RGO-CNT/PDMS	Photothermal	479 °	~ 3.6/120	133 $°s^{-1}$	80	250 mW cm^{-2}	[4]
PC/SWNT	Photothermal	90 °	~ 0.67/11	134 $°s^{-1}$	25	100 mW cm^{-2}	[9a]
CNT/PDMS	Photothermal	215 °	~ 0.83/105	259 $°s^{-1}$	-	250mW cm^{-2}	[1]
BOPP/CF	Electromagnetic	0.40 cm^{-1}	~ 0.27/90	1.48 cm^{-1} s^{-1}	-	DC 72 V	This work
BOPP/CF	Electromagnetic	0.55 cm^{-1}	~ 3/90	0.18 cm^{-1} s^{-1}	~ 50	DC 40 V	This work
BOPP/CF	Photothermal	0.75 cm^{-1}	~ 1.6/90	0.47 $cm^{-1}s^{-1}$	~ 40	230 mW cm^{-2}	This work

Supporting Information

Wireless Multi-Stimulus-Responsive Fabric-based Actuators for Soft Robotic, Human-Machine Interactive and Wearable Applications

*Rong Yin, Bao Yang, Xujiao Ding, Su Liu, Wei Zeng, Jun Li, Su Yang, Xiaoming Tao**

Dr. R. Yin, Dr. B. Yang, X.J. Ding, S. Liu, Dr. W. Zeng, J. Li, S. Yang, and Prof. X. M. Tao
Research Center of Smart Wearable Technology, Institute of Textiles and Clothing, The Hong Kong Polytechnic University, Hong Kong, P. R. China

Dr. R. Yin
Wilson College of Textiles, North Carolina State University, Raleigh, NC 27606, U.S.A.

E-mail: xiao-ming.tao@polyu.edu.hk

S1. Optimal value of m

From equation (1), we know that the curvature (κ) is proportional to c. Thus, the highest value of c is highly desirable to be achieved. The parameter c only relies on n and m, which is given below.

$$c = 6\frac{(1+m)^2}{3(1+m)^2+(1+mn)(m^2+\frac{1}{mn})} \quad \text{(S1)}$$

If we take a derivative of equation (S1) by differentiating m, one will be obtained

$$\frac{\partial c}{\partial m} = -\frac{6(1+m)^2(6(1+m)+(m^2+\frac{1}{mn})n+(2m-\frac{1}{m^2n})(1+mn))}{(3(1+m)^2+(m^2+\frac{1}{mn})(1+mn))^2}+\frac{12(1+m)}{3(1+m)^2+(m^2+\frac{1}{mn})(1+mn)} \quad \text{(S2)}$$

If $\frac{\partial c}{\partial m}=0$, $m = {}^{1}/_{\sqrt{n}}$. Moreover, the following relationship is also satisfied

$$\frac{\partial^2 c}{\partial^2 m} < 0, \text{ for } 0.01 \leq \text{n} \quad \text{(S3)}$$

Therefore, when $m = {}^{1}/_{\sqrt{n}}$, the highest value of c can be obtained.

Table S1. Parameters utilized in calculation

Symbol	Value
The CTE of the active layer, α_1	124×10^{-6} K^{-1}
The CTE of the passive layer, α_2	5×10^{-6} K^{-1}
The difference between the CTE of the active layer and that of the passive layer, $\Delta\alpha$	119×10^{-6} K^{-1}
Temperature of the fabricated temperature, T_0	22 ºC
Temperature of testing, T	22-67 ºC
Temperature change, ΔT	0 - 45 ºC
The thickness of the passive layer, t_1	35 μm
The thickness of the active layer, t_2	55 μm
The total thickness of the actuator, h	90 μm
The Young's modulus of the passive layer, E_1	1388 MPa
The Young's modulus of the active layer, E_2	785 MPa
The ratio of thickness, m	$m = t_1/t_2$
The ratio of Young's modulus, n	$n = E_1/E_2$

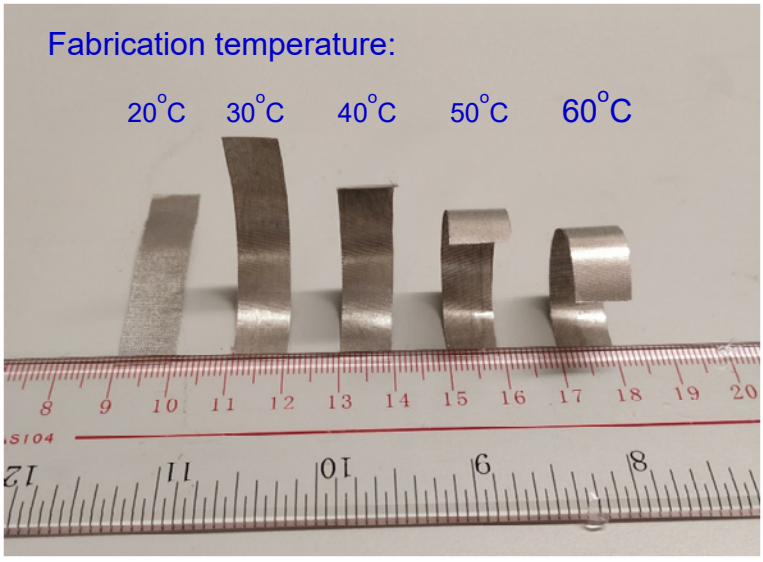

Figure S1. Different initial status at room temperature (20 ℃) of the actuators, which are fabricated at different temperature within the range from 20 ℃ to 60 ℃.

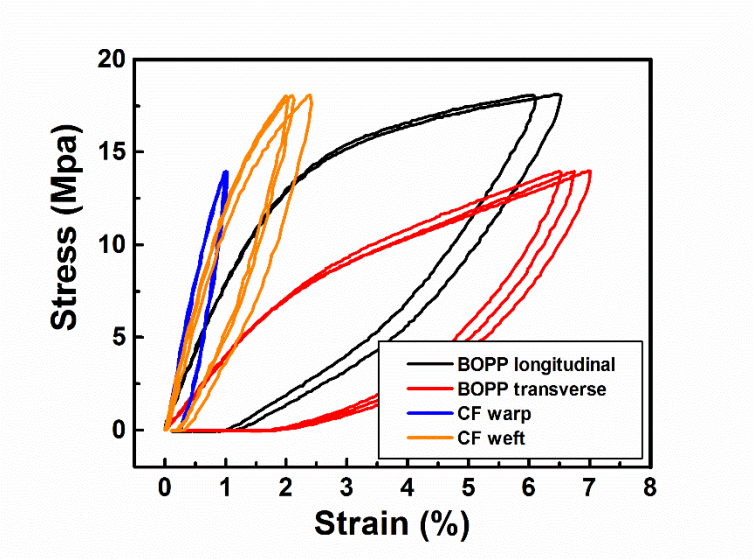

Figure S2. Three cyclic stress-strain curves of the BOPP film in the longitudinal and transverse direction and the conductive fabric (CF) in the weft and warp direction, showing a good repeatability and a good linearity at the initial stage of loading for the BOPP film (over 1.0 %) in the longitudinal direction and the conductive fabric (CF) in the warp direction (over 0.5 %).

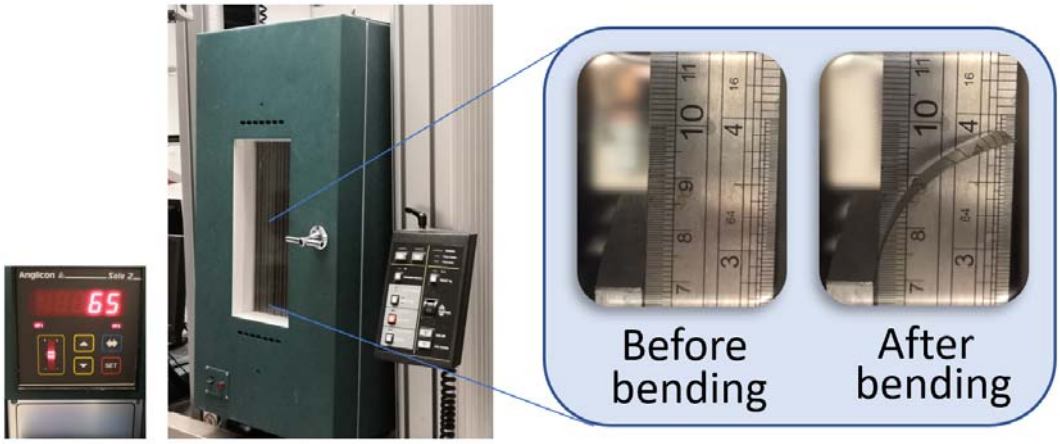

Figure S3. The chamber with an Anglicon Solo 2 controller and an illustrated sample before and after bending.

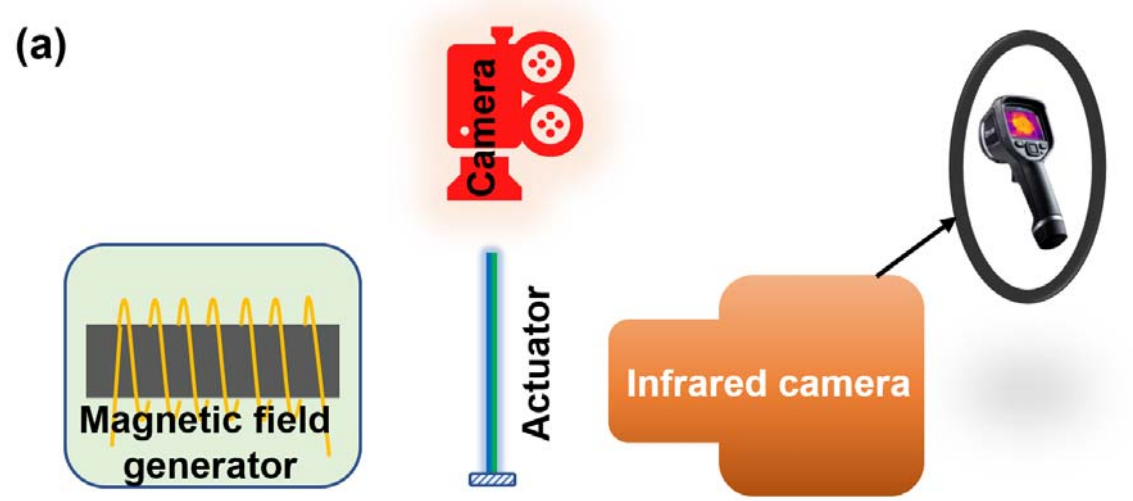

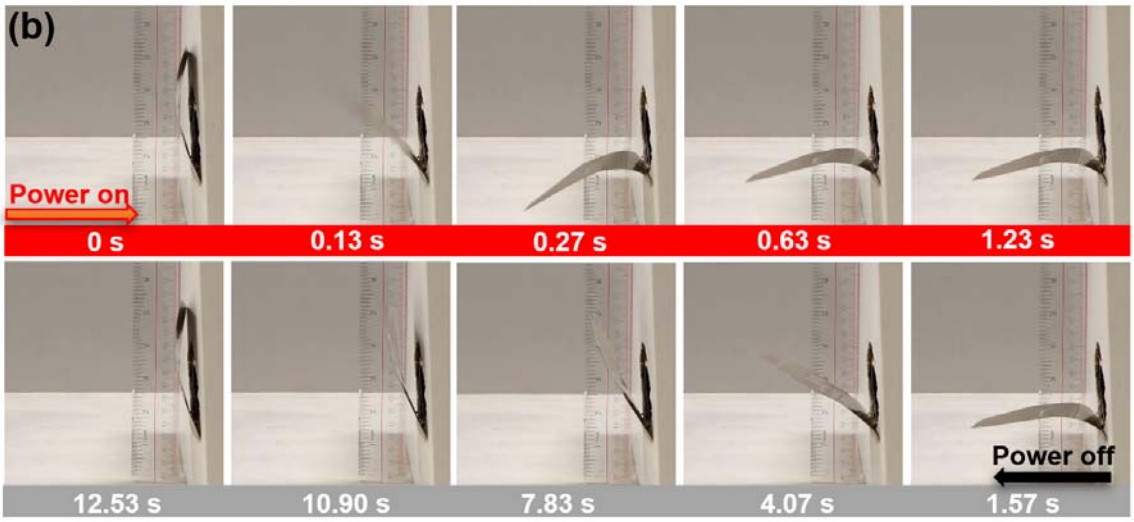

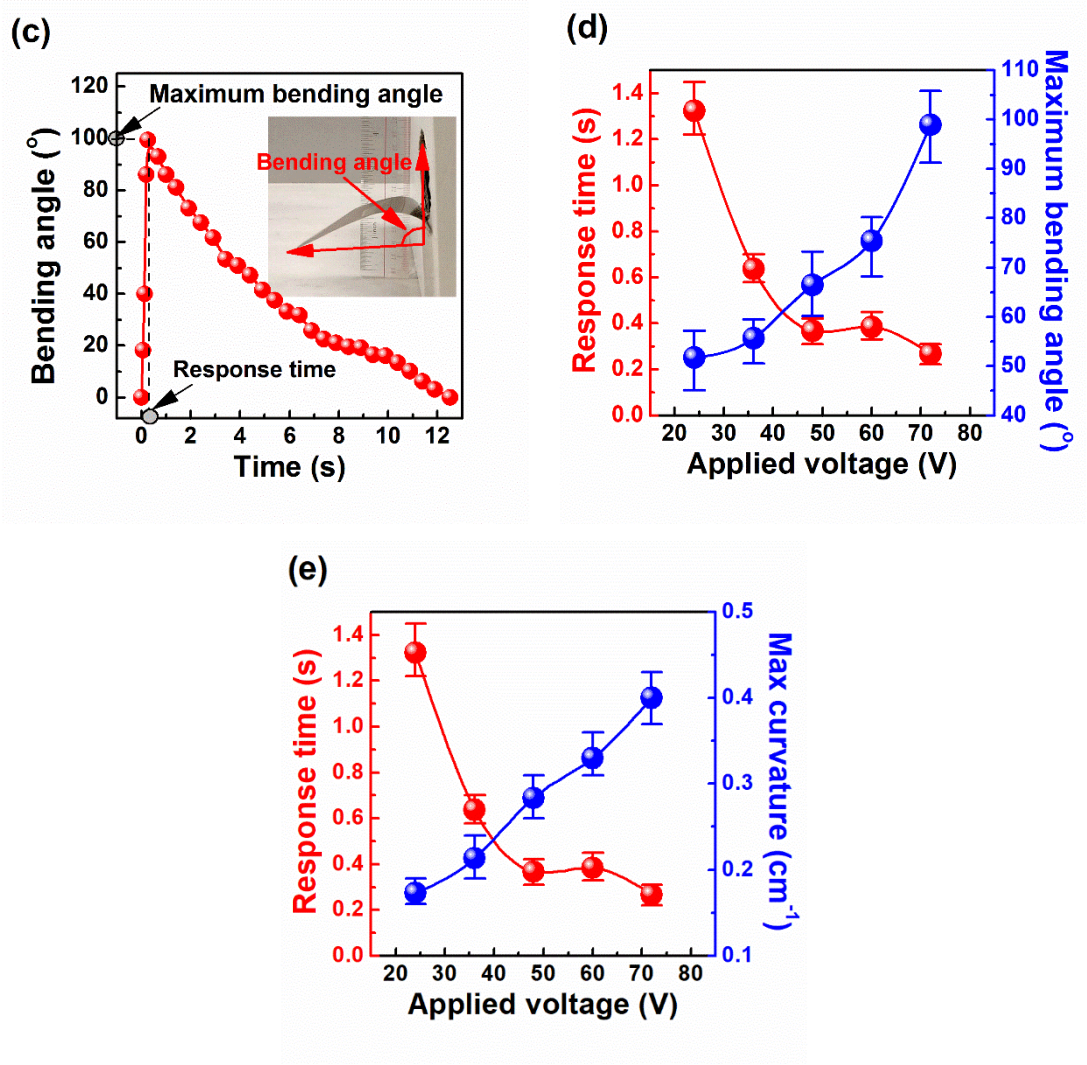

Figure S4. Actuation induced by varying electromagnetic fields. (a) Schematic of experimental setup and physical photo of devices, where the side view of the actuation process of the actuator was recorded by a camera, and the temperature distribution on the front side was recorded by an infrared camera simultaneously. (b) Electromagnetically induced actuation of a wireless-controlled actuator with 75mm in length and 45 mm in width, where the lower end of the actuator is fixed, and the input DC voltage of magnetic field generator is 72 V. (c) Corresponding bending angle of the fabricated actuator as a function of time. The inset defines the bending angle. (d) Maximum bending angle and the corresponding response time as a function of the input voltage. (e) Maximum curvature and the corresponding response time as a function of the input voltage.

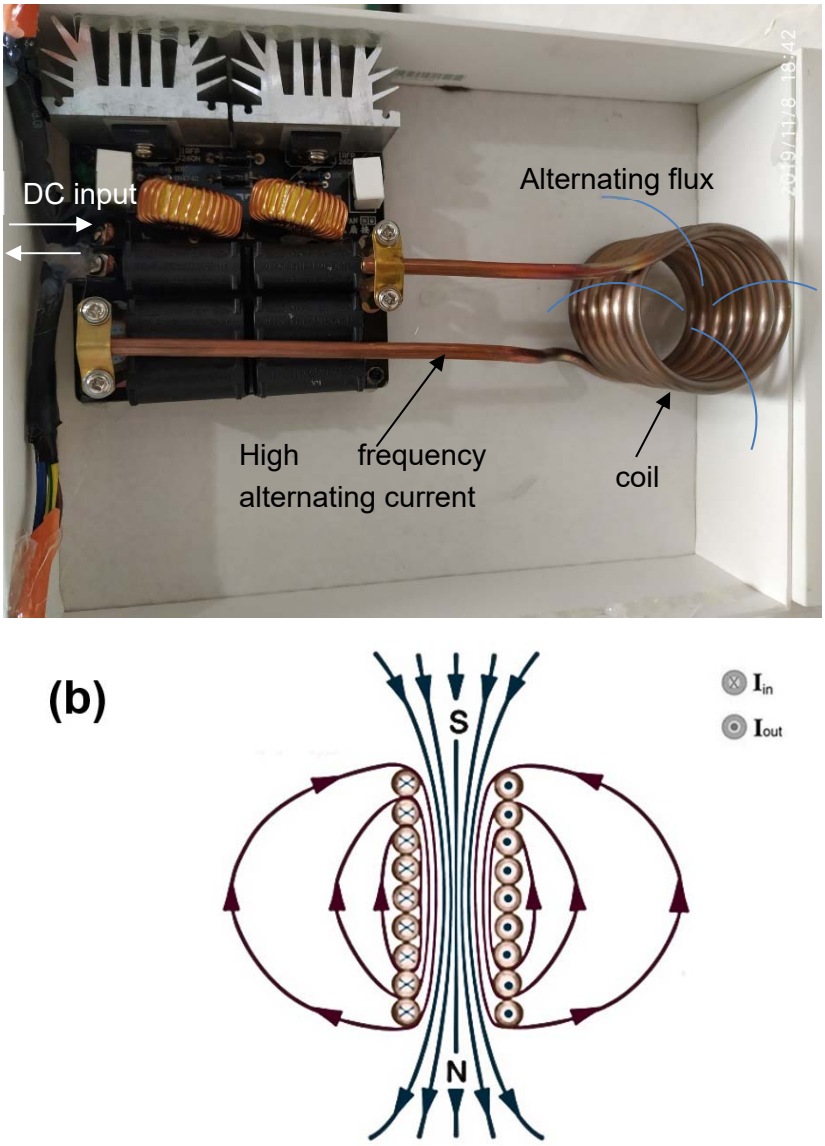

Figure S5. **(a)** Device for electromagnetic stimulation. High frequency alternating flux is generated around the coil; (b) Schematic of the magnetic field generated by the current in the solenoid.

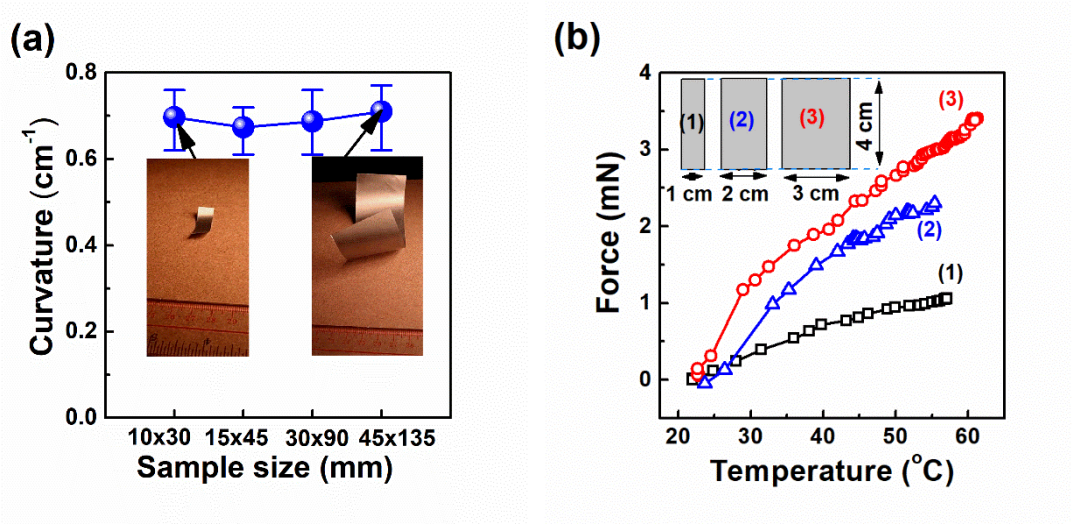

Figure S6. (a) Bending curvatures of four actuators with different scales (same length to width ratio), showing a similar curvature. (b) Blocking force of the actuators with three different widths as a function of temperature.

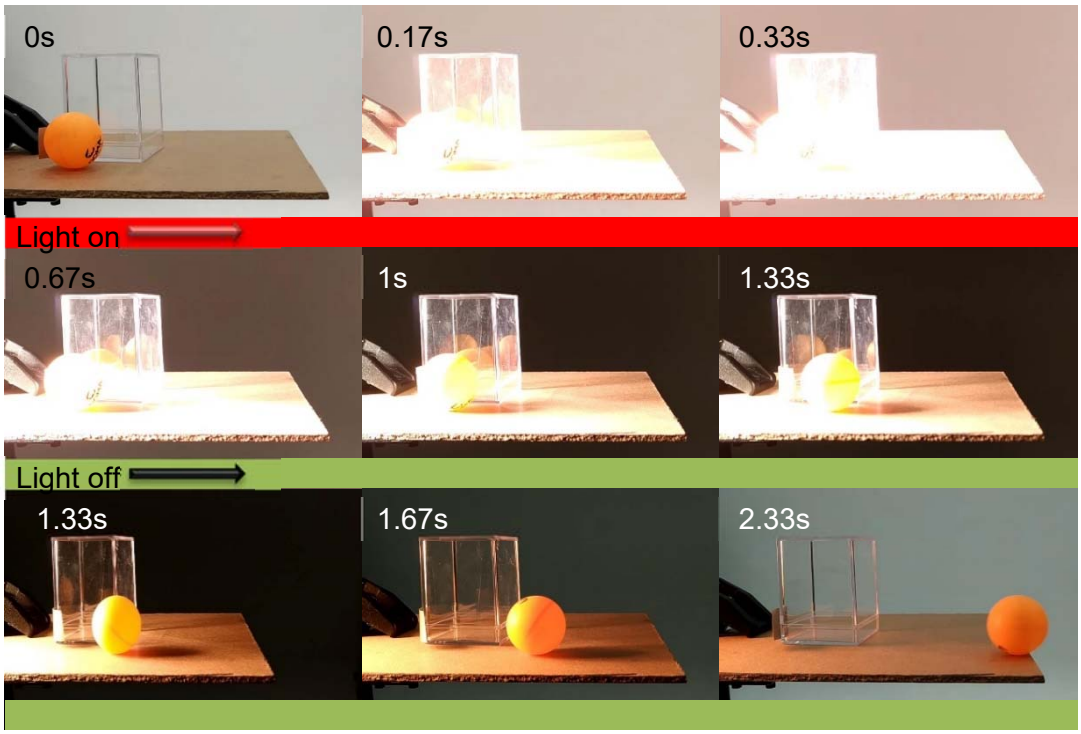

Figure S7. Optical images of a light driven soft kicker. With the light on (0 - 0.33 s) and off (0.33 s - 2.33 s), the soft robot kicks and releases a table tennis ball. The sample size was 25mm x 25mm and a light intensity of about 130 mW cm^{-2} was employed.

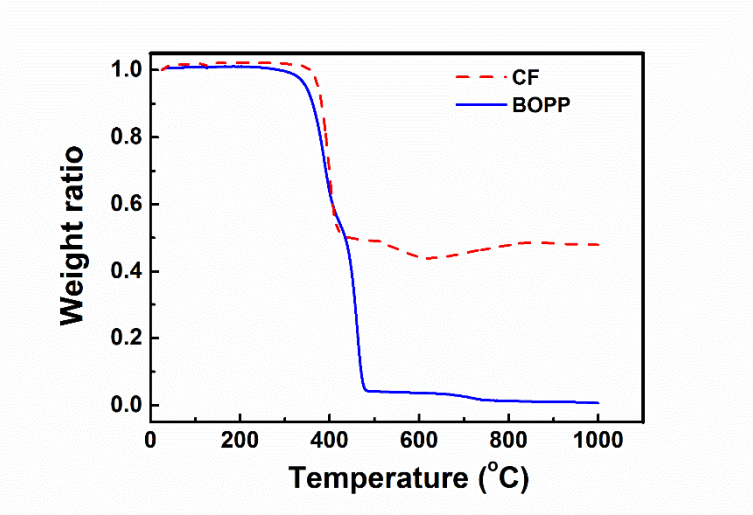

Figure S8. Thermogravimetric curves of the conductive fabric (CF) and the biaxially oriented polypropylene (BOPP) film with a thin acrylic glue layer.